



PeV proton acceleration in Gamma-ray Binaries

A.M. Bykov^{a,*}, A.E. Petrov^{a,*}, G.A. Ponomaryov^{a,b}, K.P. Levenfish^a, M. Falanga^{c,d}

^a*Ioffe Institute, Saint-Petersburg, Polytechnicheskaya str., 26, 194021, Russia*

^b*Peter the Great St. Petersburg Polytechnic University, Saint-Petersburg, Polytechnicheskaya str., 29, 195251, Russia*

^c*International Space Science Institute, Bern University, 3012 Bern, Switzerland*

^d*Physikalisches Institut, University of Bern, Sidlerstrasse 5, 3012 Bern, Switzerland*

Abstract

Current generation of ground based gamma-ray telescopes observed dozens of sources of photons above 100 TeV. Supernova remnants, pulsar wind nebulae, young stellar clusters and superbubbles are considered as possible sites of PeV-regime particles producing the radiation. Another possible source of PeV particles could be gamma-ray binary systems. In these systems, a strong relativistic outflow from a compact object (neutron star or black hole) collides with the dense wind from a massive companion early-type star. Gamma-ray binaries are observed from radio to high energy gamma-rays as luminous non-thermal sources. Apart from acceleration of very high energy leptons producing most of the non-thermal radiation, these systems may also efficiently accelerate protons. We present here the results of numerical simulation of the PeV-regime proton acceleration in gamma-ray binaries. The simulation is based on relativistic MHD modeling of local flows of magnetized plasma in the region of interaction of two colliding winds. We then inject 0.1 PeV protons into the system and directly follow their trajectories to demonstrate that they are accelerated to energies above PeV. High magnetization of the wind of the young massive star providing a Gauss range field in the winds interaction region is of paramount importance for the acceleration of protons above PeV. The maximum energies of protons accelerated by colliding winds in gamma ray binaries can significantly exceed the energy of the pulsar potential's drop, which limits from above the energy of particles accelerated by an isolated pulsar.

© 2024 COSPAR. Published by Elsevier Ltd All rights reserved.

Keywords: gamma-ray binaries; pulsar wind nebulae; MHD modeling

1. Introduction

Identification of sources of PeV particles is of great interest for the problem of the origin of cosmic rays (see, e.g., Aharonian et al., 2019; Sudoh & Beacom, 2023; Bykov et al., 2018; Amato & Casanova, 2021; Cristofari, 2021, and the references therein). Recently, the LHAASO observatory reported the discovery of 12 sources of ultrahigh-energy photons with energies up to 1.4 petaelectronvolts (Cao et al., 2021). The source of the highest energy photon – 1.4 PeV photon LHAASO J2032+4102 – is located in the Cygnus region, which is very rich in potential cosmic ray accelerators. Real candi-

dates for accelerators include the young massive stars Cyg OB1 and OB2, the microquasars Cyg X-1 and Cyg X-3, the supernova remnant γ -Cygni, the Cygnus Cocoon, and gamma-ray binaries (see e.g. Aharonian et al., 2002; Ackermann et al., 2011; Abeysekara et al., 2018, 2021; Tibet AS γ Collaboration et al., 2021). One of the gamma-ray binaries – PSR J2032+4127 – is consistent in position with the source LHAASO J2032+4102. This indicates the need for theoretical modeling of gamma-ray binaries as potential sources of protons in the multi-PeV range. The results of such modeling are presented in this paper.

Galactic magnetars and millisecond pulsars are considered for the role of particle accelerators up to energies above PeV (e.g. Arons, 2003, 2012; Kotera et al., 2015; Lemoine et al., 2015; de Oña Wilhelmi et al., 2022). Recently, Guépin et al. (2020) performed a detailed 2D particle-in-cell modeling of the acceleration of protons extracted from the surface of a neutron

*Corresponding author

Email addresses: byk@astro.ioffe.ru (A.M. Bykov),
a.e.petrov@mail.ioffe.ru (A.E. Petrov)

star-pulsar with an axisymmetric magnetosphere. Their simulations took into account production of pairs and the magnetic field structure in the pulsar's magnetosphere, in which protons are accelerated in separatrix current layers inside the light cylinder of the pulsar. The highest energies, that protons in the model can reach, exceed 10% of the total vacuum potential drop, and the luminosity can be several percent of the pulsar spin-down luminosity. General considerations have led de Oña Wilhelmi et al. (2022) to the following estimate for the maximum energy E_{\max} that particles (electrons or protons) accelerated by an isolated rotating pulsar with spin-down power \dot{E} can receive:

$$E_{\max} \approx 2 \eta_e \eta_B^{0.5} \dot{E}_{36}^{0.5} \text{ [PeV]}. \quad (1)$$

Here η_e is the ratio of the electric and magnetic field strengths at the pulsar wind termination surface, $\eta_B \leq 1$ is the wind magnetization parameter, and \dot{E} is measured in units of $10^{36} \text{ erg s}^{-1}$.

The pulsars in binaries can accelerate particles to energies well above the limit given by Eq.1 in the region where the pulsar wind collides with the wind of the companion star. The region where two MHD flows collide is known to be a favorable place for particle acceleration (see e.g. Eichler & Usov, 1993; Tavani & Arons, 1997; Bykov et al., 2012; Bosch-Ramon, 2013; De Becker & Rauq, 2013; Bykov et al., 2017; Grimaldo et al., 2019; Molina & Bosch-Ramon, 2020; Vieu et al., 2020; Pittard et al., 2021; Malkov & Lemoine, 2023; Abaroa et al., 2023). If the companion's wind is magnetized strongly enough to confine efficiently PeV particles in the system, those binaries could potentially accelerate particles to multi-PeV energies.

Such a system can be well represented by the gamma-ray binary PSR J2032+4127/ MT91 213, which is considered as a possible identification for the PeV source LHAASO J2032+4102. The binary is hosting a pulsar with a very eccentric orbit. The estimated orbital period is about 45–50 years (Ho et al., 2017). The pulsar has a spin period of about 143 ms, and an estimated spin-down power about $1.5 \times 10^{35} \text{ erg s}^{-1}$. This spin-down power is almost an order of magnitude less than that would be required for an isolated pulsar to accelerate protons to PeV energies (see Eq. 1). In this regard, de Oña Wilhelmi et al. (2022) pointed out that among the 11 very high-energy LHAASO sources which could be identified with some pulsars, only PSR J2032+4127 have a problem with such an identification when considering the particle acceleration mechanisms available to isolated pulsars. However, in the gamma-ray binary PSR J2032+4127/ MT91 213 particles accelerated in the pulsar vicinity can substantially increase their energy even further in the colliding winds flow. Monte Carlo simulation of colliding winds in the binary system PSR J2032+4127/MT91 213 under simplifying assumptions about their structure showed that for particles to reach PeV energies, a strong Gauss-range magnetic field in the wind of the massive companion-star is required (Bykov et al., 2021). From the observational side, dipole fields exceeding 100 G are found in about 10% of massive O, B, A type stars (Grunhut et al., 2017; Shultz et al., 2019), and many of Be type stars have magnetic field in the kG range. Furthermore, Hubrig et al. (2023) found that massive stars in binary and multiple systems (the progenitors of gamma-ray binaries)

are more likely to have strong magnetic fields. The wind of such massive star in a binary should also carry a strong field.

In this work, we are focusing on the very ability (or inability) of pulsars in gamma-ray binaries to accelerate ions above the limit given by Eq. 1 and namely to energies of $\sim 10 \text{ PeV}$ in PSR J2032+4127. To this end, we carried out a relativistic magnetohydrodynamical (RMHD) simulation of a pulsar wind nebula (PWN) which is interacting with the fast magnetized wind of a massive companion star, supplemented with a module (unit) for tracking the trajectories of accelerating ions (considered as test particles) inside the system. Our simulation takes into account the effect of the Gauss-range magnetic field of the dense wind of a massive early-type star on the PWN's structure, evolution and particle acceleration. Such a field can greatly affect both the acceleration and propagation of high-energy particles in the system, allowing gamma-ray binaries to become bright in the PeV range.

2. Model description

Gamma-ray binaries consist of a massive early-type star and a compact object, a neutron star-pulsar or a black hole. A dozen of such gamma-ray loud objects, observed from radio to high-energy gamma-rays, are known for their high gamma-ray luminosity (for a review, see, e.g., Dubus, 2013; Romero et al., 2017). Multi-wavelength observations of gamma-ray binaries at different orbital phases (e.g., Abeysekara et al., 2018; Ng et al., 2019; Hare et al., 2019; Chernyakova et al., 2020b) laid the foundation for a numerical study of their structure and radiation (e.g., Takata et al., 2017; Chen et al., 2019; Huber et al., 2021; Fiori et al., 2022).

The binary systems with a pulsar – such as PSR J2032+4172, PSR B1256-63 and, likely, LSI +61° 303 – power two colliding flows: the wind of a massive star and the relativistic wind of a pulsar. In this work we are interested in systems in which a young massive star of early-spectral class O or B (e.g. Tavani & Arons, 1997; Torres, 2011) is orbited by a rotation-powered pulsar. Rotation-powered pulsars are known for their ability to inflate a fairly energetic pulsar wind nebula. The interaction of the nebula with the dense, highly magnetized wind of a massive star is of interest for the problem of cosmic ray acceleration.

There are three specific features which distinguish a pulsar nebula in gamma-ray binaries from one created by an isolated pulsar. In the binaries, the nebular outflows are exposed to the intense radiation field of the young star. Ball & Kirk (2000) studied whether such radiation could slow down the pulsar wind (in the generic case of the gamma-ray binary PSR B1259-63) due to the inverse Compton drag force and found that the effect is insignificant. The second feature is the orbital motion of the pulsar in the binary. The motion can affect the structure of the region where the winds of the companions collide. A thorough modeling of colliding winds in binaries was carried out by Lemaster et al. (2007) and Bosch-Ramon et al. (2012) who studied the effect of the Coriolis force on the PWN dynamics. The third feature is the strong (Gauss-range) magnetic field of the wind of the massive star. Such a strong field has a profound

effect on the structure and dynamics of the nebular outflows and their very ability to accelerate particles above PeV energies, the latter being the main goal of our study. Considering that the force of radiative braking is insignificant, let us evaluate the relative role of two other forces affecting the plasma dynamics in the colliding winds – magnetic and Coriolis. We consider the structure of the wind collision region in the rest frame of the pulsar. The pulsar moves with an angular velocity Ω along the Keplerian orbit. In the pulsar's frame, the density of the Coriolis force applied to a plasma element of mass density ρ is represented by the term $-2\rho\Omega \times \mathbf{u}$. In turn, the magnetic force density is given by the term $[2(\mathbf{B}\nabla)\mathbf{B} - \nabla B^2]/8\pi$. The relative role of the forces can be evaluated through the parameter $\xi = 8\pi\rho\Omega R u/B^2$. Expressing the Keplerian frequency Ω through the mass of the young star (M), and the plasma density of the stellar wind (the one of the pulsar wind is much lower) through the mass loss rate (\dot{M}), one can obtain

$$\xi \approx 0.05 M_{10}^{1/2} \dot{M}_{-7} R_{12}^{-1/2} B_2^{-2}, \quad (2)$$

if one assumes the equatorial supersonic stellar wind with the Parker-type magnetic field structure. In the latter case, the magnetic field in the equatorial disk scales as $\sim R^{-1}$, so the surface magnetic field above 100 G would provide the stellar wind field $B_{sw} \sim \text{Gauss}$ at the separation distance of 10^{14} cm. In turn, ξ scales with the distance from the young star as $R^{-1/2}$. In the equation above, M is measured in units of $10 M_{\odot}$, \dot{M}_{-7} in $10^{-7} M_{\odot} \text{ yr}^{-1}$, R_{12} in 10^{12} cm, and the dipole magnetic field B_2 at the stellar surface is in 100 G.

The relative role of the forces varies along the pulsar orbit. Estimates of the mass-loss rates of O and early B stars (obtained from a sample of 67 stars) range from $\dot{M}_{-7} \sim 1$ for O-type stars, to $\dot{M}_{-7} \sim 0.01$ – 0.1 for B0–B3 type stars (Kobulnicky et al., 2019). At the periastron distance ($\sim \text{AU}$) of the gamma-ray binaries known to host a pulsar, the influence of the Coriolis force may be relatively weak provided that the massive star's wind at this distance has a field in the Gauss range. To estimate the extent of the structured magnetic disk of rapidly-rotating Be-stars Ressler (2021) used MHD simulations and found the disk extension to be several tens of the massive star radii that gives $\sim \text{AU}$ for typical radii values $\sim 10^{12}$ cm. Thus, at the periastron stage of the orbit high Gauss-range magnetic field provided by the equatorial disk may reach the vicinity of the pulsar. This allows to neglect the effect of the Coriolis force on the plasma flows structure in the colliding winds region and provides conditions for protons acceleration to multi-PeV energies. Interestingly, the time to accelerate PeV proton in the PWN – stellar wind collision region with the Gs-range field is a few hours. This sets the natural time period of simulation of PWN with the colliding winds structure to be about a day.

Our relativistic MHD model comprises three components: (i) the stellar wind, (ii) the pulsar wind, and (iii) the test-particle relativistic cosmic rays interacting with the plasma flows of the colliding winds. The model components used in numerical simulations are described in Appendixes. The choice of the model parameters (listed model-by-model in the legend to Table 1) is explained below.

(i) The massive star's wind. Hot, rapidly rotating Be-stars may form an equatorial disk of rotating plasma (Rivinius et al., 2013). An extent of such structured magnetic disk is difficult to infer from observations, but MHD simulation by Ressler (2021) gives it an estimate of several tens of stellar radii. On the surface of Be-stars, the magnetic field can reach several kiloGausses (Shultz et al., 2019). Such a strong field can seriously influence the structure and dynamics of the radiatively driven stellar wind (ud-Doula & Owocki, 2022), especially in the equatorial disk. The magnetization of the plasma there can be so strong that it will channel the flow into a field-aligned configuration.

In the case of the gamma-ray binary PSR J2032-4127 – MT91 213 (see Ho et al. (2017) for its orbital parameters) three years after the passage of periastron the pulsar in this system was observed at a separation distance of $R \sim 20$ AU from a massive Be-star and could pass through its equatorial disk according to the model by Klement et al. (2017). The magnetic field could be of several Gauss if it decreased in the equatorial disk as $\sim 1/R$ from the value of several kG on the surface of the Be-star. So, we assumed that at this stage of the orbit the stellar wind had a magnetic field B_{sw} of several Gauss, a flow velocity $v_{sw} \sim 300 \text{ km}\cdot\text{s}^{-1}$, and a number density $n_{sw} \sim 3 \cdot 10^4 \text{ cm}^{-3}$ in the vicinity of the pulsar orbit. The reference values taken above are consistent with the stellar wind models by Klement et al. (2017) A wind with such parameters could be magnetically governed at distances of up to hundreds of stellar radii, as can be seen from a comparison of its magnetic and ram pressures, $B_{sw}^2/8\pi$ and $\rho_{sw}v_{sw}^2/2$.

Being interested in the orbital phases where PeV proton acceleration is expected we place a pulsar wind nebula to develop within a dense, highly magnetized, disk-like stellar outflow with a field-aligned configuration. To simplify the numerical simulations over the time periods of a day duration the wind of massive companion star was approximated asymptotically away from PWN as a stationary, homogeneous flow of given pressure and density. The magnetic field and bulk velocity are co-directional and have a fixed direction relative to the pulsar rotation axis. Note that in this case protons can boost their energy mostly in the vicinity of the pulsar wind nebula since the simulated stellar wind is asymptotically homogeneous. In more realistic case of a clumpy stellar wind PeV particle acceleration is even more efficient. The stellar wind velocity v_{sw} is actually the velocity of the pulsar relative to the stellar wind, because we are considering the system in the pulsar rest frame. The speed of the pulsar in orbit is tens to hundreds $\text{km}\cdot\text{s}^{-1}$, so any value of v_{sw} of this order seems to be reasonable. The stellar wind model parameters are listed in Table 1. There ψ represents the angle between the \mathbf{B}_{sw} and the pulsar's rotation axis. Here we take $\psi = 45^\circ$ to illustrate the effects and defer analysis of the consequences of this choice until a dedicated study.

(ii) The pulsar wind model, the second component of our model system, is described in details in Appendix B. The model was introduced in Porth et al. (2014) and now is widely used in simulating pulsar wind nebulae (for references see, e.g., Porth et al., 2017). As stated above we place our model pulsar wind nebula to develop within a dense, highly magnetized stellar wind. Under these conditions, the nebula turns out to be much

more compact than it would be if it were developing inside an evolved supernova remnant. As a result, it quickly develops its characteristic flow pattern. For the nebula, this takes no more than a few hours, even if it is inflated from a scratch (which is the case in all our runs). Then high energy cosmic ray particles injected there can be effectively upscattered and further accelerated by magnetic inhomogeneities which are carried by the mildly relativistic flows in the vicinity of the pulsar wind termination shock.

(iii) Test-particle protons of PeV energies are the third component of our model system. We demonstrated below that the relativistic ions can increase their energy to ~ 10 PeV in just a few successful head-on collision with magnetic inhomogeneities of mildly-relativistic velocities. Scatterings on the fast moving magnetic inhomogeneities revealed in our simulations (see Fig.2) – which have spatial scales of about PeV particles gyroradii and move with Lorentz-factors $\Gamma > 3$ – are especially efficient. Since the acceleration process occurs locally in the vicinity of PWN and takes only $\sim 10^5$ sec, it is practically independent of the system's pre-history. That is, PeV protons care little about the structure that the nebula had in parts of the pulsar orbit other than where their acceleration began. PeV protons also have little regard to the symmetry of the system. For them, only the spatial scale of the acceleration site and the spectrum of its magnetic inhomogeneities are important. Recall again, that in this study we are modeling the very ability of the pulsars with $\dot{E} > 10^{35}$ erg s $^{-1}$ in binaries to accelerate particles to multi-PeV energies.

Since the acceleration of PeV particles is practically insensitive to the symmetry and the structure of flows far away from the acceleration site, we simulated the system of two colliding winds in a planar 2D geometry. This choice is motivated by the excessively large computational resources that would be required for 3D modeling of propagation of particles in time-dependent MHD flows. To trace the trajectories of accelerated particles, the plasma flow simulations must have a numerical grid that covers a wind collision region of tens of AU in size and simultaneously resolve the spatial scales on the order of sub-PeV particle gyroradii (~ 0.02 AU for a 0.1 PeV proton in a field of 1 G).

Concluding the description of the model, we once again emphasize that the processes of interest to us here is the acceleration of multi-PeV particles. Both particle acceleration process and the adjustment of PWN's flows to the colliding stellar winds condition have similar time scales of the order of a few hours. This is short compared to the time of the orbital revolution of pulsars in most of the gamma-ray binaries of interest which are ~ 26 days for LSI +61 $^{\circ}$ 303, ~ 3.4 yr for PSR B1259-63, and ~ 45 –50 yrs for PSR J2032-4127 (Shannon et al., 2014; Ho et al., 2017).

3. Results

We conducted a series of numerical experiments with different stellar wind magnetic fields (B_{sw}) to study their influence on the ability of gamma-ray binaries to accelerate protons well above PeV. In Figs. 1–3 we show the pattern of flows which is

formed in a pulsar wind nebula under the influence of a highly magnetized stellar wind. The pattern is characteristic of a fully inflated nebula and develops just a few hours after the nebula begins to inflate, for any of B_{sw} under consideration. Again, this is much shorter than the orbital revolution of a pulsar. It seems to be a reasonable approximation even for the system LS 5039 with the shortest known orbital period of 3.9 days (Casares et al., 2005). Therefore, this justifies considering the local structure of the wind collision system (i.e., considering a nebula in a short local part of the orbit) and fixing the directions of \mathbf{B}_{sw} and \mathbf{v}_{sw} on the simulation time scale, which is what we do in our simulations.

3.1. Local structure of the wind collision region

Fig. 1 visualizes the local structure of the wind collision region and its change due to an increase in B_{sw} . Four panels in the figure illustrate cases with $B_{sw} = 0.1, 1, 2$ and 3 G. In the dense stellar wind, a PWN creates a cavity of characteristic dimensions of several AU. This is much smaller than what the same nebula would create if its pulsar were isolated and surrounded by the tenuous plasma of a supernova remnant. In a smaller cavity, magnetic field energy accumulates much more rapidly. By the time the nebula is fully inflated, its fields reach the sub-Gauss range (which is high compared to the tens or hundreds of μ G for the fields of PWNe in supernovae). Reducing the size of the nebula and enhancing its magnetic irregularities help increase the efficiency of accelerating high-energy particles in the system (Fig. 4).

The stellar wind surrounding the nebula may have an even stronger field: $B_{sw} \sim$ Gauss. A strong field modifies the region of wind collision in several ways. Foremost, it most likely begins to control the structure and dynamics of the wind itself. As B_{sw} increases, there is more and more reasons to expect that the velocity field and magnetic field of the wind become co-directional. Second, the strong field reshapes the pulsar wind nebula, noticeably narrowing it across the field direction and slightly stretching along this direction (see Fig. 1). When B_{sw} reaches ~ 3 G, the nebula becomes nearly 3 times narrower in the transverse direction, than in the longitudinal. At the same time, the total volume of the wind collision region practically does not change with increasing B_{sw} . At sub-Gauss fields, almost all of this volume is occupied by the PWN itself. As the field strengthens, the nebula gives up more and more of this volume to a kind of dense cocoon that forms around it from the plasma of the massive star wind. Along most of the perimeter of the nebula, the plasma in the cocoon turns out to be several times denser than the plasma outside the collision region. As a result, the field in the cocoon is several times greater than the field outside. Even if the latter is in the sub-Gauss range, the cocoon field will still be \sim Gauss. Clearly that wrapping the nebula in a magnetic cocoon is of paramount importance for confining and accelerating particles of ultra-high energies within the region of wind collision. This importance becomes even greater if we notice the development of magnetic inhomogeneities in the cocoon, which appear despite the fact that the wind outside the cocoon is assumed to be completely uniform in our runs.

Fig. 2 characterizes the collision region from a slightly different aspect (model C in Table 1). There we show a map of flow velocity, in units of c in the upper panel and in units of the Lorentz factor Γ in the lower panel. The map shows signs that in the windward side of the region, mildly relativistic flows may occupy a larger part of the available volume than in the leeward side. In the lower panel we zoom in on the surroundings of the wind termination shock. There, for clarity, a contour plot of the Lorentz factors is superimposed on a gray-color map of magnetic field magnitudes. The panel demonstrates the presence in the system of mildly-relativistic magnetized flows with $\Gamma \lesssim 3$, as well as individual magnetic clumps with even higher $\Gamma \sim 4.5$ and with characteristic sizes comparable to the gyro-radii of PeV-regime particles.

3.2. High energy particle acceleration

Proton gyroradii scale with magnetic field strength as $R_g \approx 3 \times 10^{12} \cdot E \cdot B^{-1}$ cm, with proton energy E measured in PeV and B in Gauss. Accordingly, fields in the Gauss-range are necessary to confine particles with energies of several PeV in the collision region of several AU in size. Then the acceleration time and the spectral energy distribution of the test particles will be determined by the broad-band spectrum of magnetic fluctuations in the acceleration region. Due to the limited numerical resolution of our experiments (aimed at simulating the trajectories of the PeV-regime particles), we cannot trace these fluctuations down to scales resonant for GeV-regime particles. Therefore, we cannot consider fluctuations over a range of scales which is wide enough for kinetic or Monte Carlo modeling of the spectral energy distribution over many decades (see e.g, Blandford & Eichler, 1987; Bykov et al., 2017). In this regard, we will limit ourselves to studies of the propagation and acceleration of test-particle protons of PeV energies.

A test-particle proton injected into the region of two colliding winds is shown in Fig. 3. The figure visualizes how this proton changes its energy as it wanders within the region. To guide the eye, the proton's trajectory is superimposed on a still map of the region's magnetic fields. Note that the choice of initial energy for an injected particle is limited both from below and from above. From below, it is bounded by the adopted resolution of the numerical grid. However, if lower energy (TeV-regime) particles were injected into our system, they would be successfully confined and accelerated, although much higher resolution runs are needed to allow RMHD flows to effectively scatter such particles. From above, the initial energy is bounded by the maximum particle energy available in the source of injection. This source can be associated either with the colliding winds region or with the termination surface of the pulsar wind (see, e.g., Amato & Arons, 2006). In the later case the initial particle energy is limited by the drop in electric potential between the pulsar and infinity (for a review, see Arons, 2012). According to a recent detailed discussion of particle acceleration by young bright pulsars in de Oña Wilhelmi et al. (2022), for protons to reach a PeV energy, a pulsar spin-down luminosity about 10^{36} erg s^{-1} is required. In gamma-ray binaries, the energy of injected proton can be further boosted in the region of winds' collision.

In Fig. 3 thick circles visualize the proton's trajectory, and their color represents the proton's energy. It can be seen that the particle reached about 14 PeV when it left the acceleration site. In our simulations, we traced trajectories of many thousands of protons, injected with different initial energy at different locations. The figure just illustrates the system's ability to confine multi-PeV protons and accelerate them above 10 PeV. This acceleration typically occurs in literally 2–3 successful up-scatterings on fast-moving magnetic inhomogeneities with the Lorentz-factors $\Gamma \gtrsim 3$ (see in Fig. 2). Indeed, a head-on collision with the plasma inhomogeneity moving with Lorentz-factor Γ may boost the particle energy in $\sim \Gamma^2$ times, like it happens with the photons undergoing the inverse Compton scattering. Such mildly relativistic plasma structures are present in the downstream of oblique parts of the pulsar wind termination shock.

Fig. 4 shows the spectral energy distributions of accelerated particles obtained in models "E" to "I" in Table 1. The upper panel illustrates how the stellar wind field B_{sw} affects the particle spectra (formed some time t after the particles were injected into the system). As mentioned in §3.1, high-magnitude fields B_{sw} help accelerating particles stay longer in the acceleration region and encounter stronger magnetic irregularities there. All this promotes acceleration. As B_{sw} increases, particle spectra become harder, and the maximum energy achieved by accelerating protons grows. The lower panel illustrates how particle spectra evolve with time. It can be seen that particles injected into the system with an initial energy of 0.1 PeV are quickly accelerated (in a few hours) to PeV energies. On the simulation timescale, particle spectra become increasingly hard.

4. Discussion

Currently, among the known gamma-ray binaries, there are two systems that definitely contain a pulsar, and one that is highly likely to contain. The pulsar PSR J2032+4127 orbits the massive companion Be-star MT91 213 (BOVp) in about 45–50 years. At periastron, the pulsar passes at a distance of $\sim 10^{13}$ cm from the Be-star. This is close enough for the pulsar wind nebula to find itself in a stellar wind magnetic field of \sim Gauss magnitude, provided the star has a surface magnetic field $\gtrsim 100$ Gauss. A rapidly rotating Be-star may also form an equatorial disk of rotating plasma (Rivinius et al., 2013). The extent of such a disk is still difficult to constrain observationally. Using MHD modeling, Ressler (2021) estimated the extent of the structured magnetic disk to be several tens of the massive star radii. If this is indeed the case, the gamma-ray binary PSR J2032+4127 may well be a plausible counterpart to the LHAASO source J2032+4102. The other two gamma-ray binaries hosting a pulsar have much shorter orbital periods. In the first one, the pulsar PSR B1259-63 with a spin-down luminosity of 8×10^{35} erg s^{-1} orbits the (apparently) Be star LS 2883 with a disk every 3.4 years (see e.g. Chen et al., 2019; Chernyakova et al., 2020a). The periastron and apastron distances of the pulsar's orbit are 1 AU and 13.4 AU, respectively (Dubus, 2013). In the second system, the gamma-ray binary LSI +61° 303, a compact object (possibly a pulsar; Weng et al.,

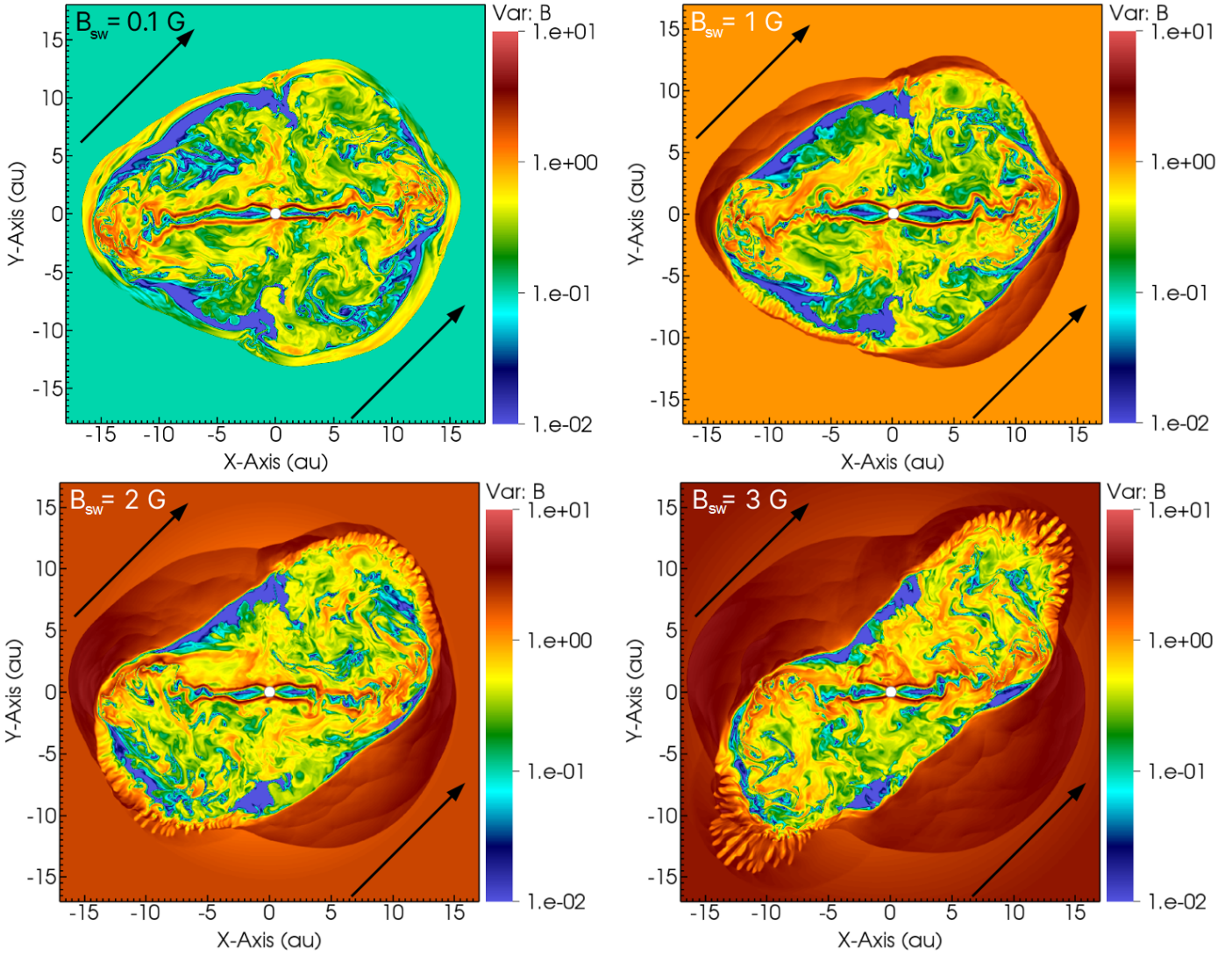


Fig. 1. Local structure of the region where two winds collide: the wind of a pulsar and the wind of a massive star. Each panel of the figure shows a map of the local magnetic field B [G] in the region. The four panels differ in the strength of the stellar wind magnetic field: $B_{sw} = 0.1, 1, 2$ and 3 Gauss (models $A-D$ in Table 1). The white circles indicate the pulsar position, while the massive star is located outside the computational domain. The black arrows indicate the direction of B_{sw} . It is oriented at an angle $\psi = 45^\circ$ to the pulsar’s rotation axis (the latter is directed upward in the maps). The pulsar wind nebula in the figure is $t = 0.56$ days old. Note that the brightness scale of the color bar is adjusted to highlight the structure of MHD flows and does not reflect exactly the maximum and minimum values of B in the region.

2022) orbits B0 Ve star in about 26.5 days. Its apastron distance is estimated to be ~ 1 AU. This binary exhibited a strong flaring activity in TeV-range photons lasting about a day around the apastron position (Archambault et al., 2016). Clearly, in the three gamma-ray binaries mentioned above, pulsar wind nebulae have to evolve in a markedly different environment compared to that can be observed around the nebulae of isolated pulsars in supernova remnants or in the interstellar medium (see e.g. Gaensler & Slane, 2006; Reynolds et al., 2017). The region of two colliding MHD flows in these systems provides favorable conditions for efficient acceleration of particles to energies well above PeV and their more intense high-energy radiation, which distinguishes gamma-ray binaries from the broader population of X-ray binaries. This may resolve the problem of the association of the gamma-ray binary PSR J2032+4127/MT91

213 with the 1.4 PeV photon source LHAASO J2032+4102.

Using the RMHD code PLUTO (Mignone et al., 2007, 2018) we modeled the wind collision region in which PeV protons can boost their energy. Our simulations revealed the character of plasma flows, including their magnetic and velocity fields, in the vicinity of the pulsar on a spatial scale smaller than the distance between the stars. The resolution of the applied numerical grid was suitable for studying the confinement and acceleration of very high energy particles of PeV regime. At pulsar spin-down rates of $10^{35} - 10^{37}$ erg·s $^{-1}$ and Gauss-range stellar wind fields, a typical pulsar wind nebula acquires an elongated shape. It turns out to be ~ 10 AU in extent in the field direction and noticeably smaller across. This is roughly 3 orders of magnitude smaller than what the corresponding nebula would be if its parent pulsar were propagating at subsonic speeds in a supernova

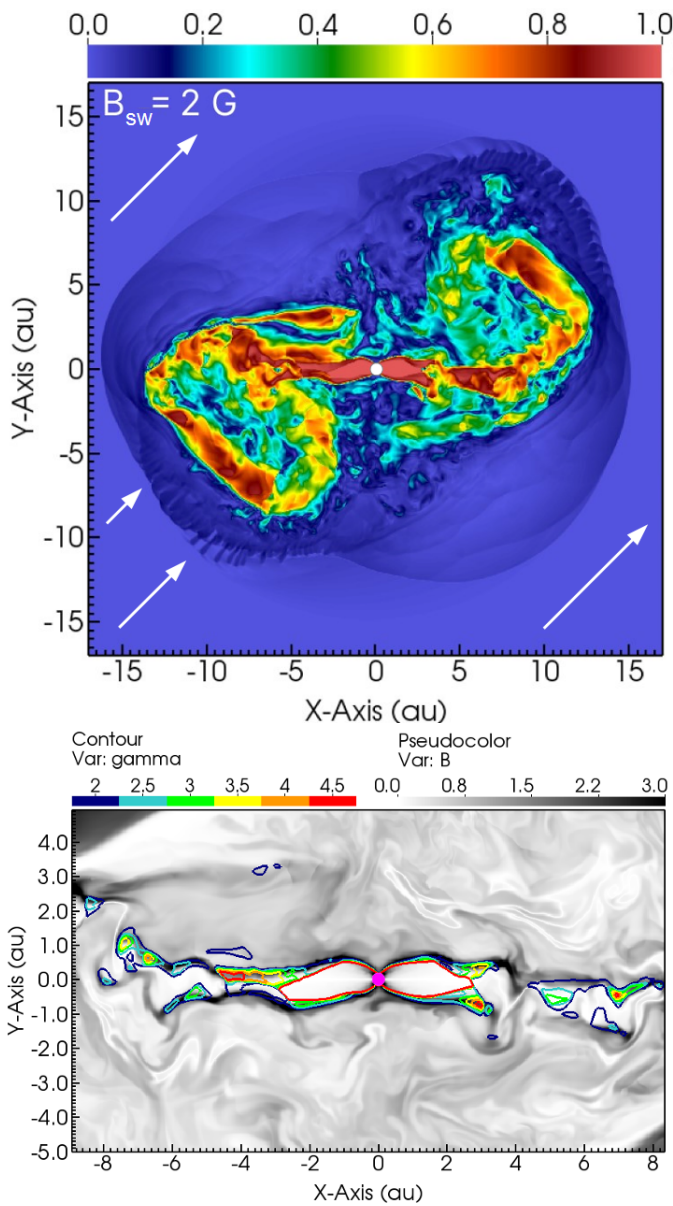


Fig. 2. Local structure of the wind collision region. A model with a stellar wind field of 2G and a pulsar spin-down luminosity of $10^{37} \text{ erg} \cdot \text{s}^{-1}$ is presented (model C from Table 1). Top: Map of flow velocity magnitude (in units of the light speed c). White arrows indicate the direction of the stellar wind flow. Note that on the windward side of the nebula, high-velocity outflows occupy more of the available volume than on the leeward side. Bottom: Contour map of the Lorentz factor of flows, Γ . The map is superimposed on a gray-color map of the local magnetic field B (in G). The $\Gamma = 4.5$ contour (shown in red), outlining the region of the pulsar's unshocked wind, practically coincides in position with the wind termination shock due to an abrupt deceleration of the wind. The brightness scale of the gray colorbar is adjusted to highlight the structure of RMHD outflows and does not reflect the maximum and minimum values of B . The nebula in the figure is 0.56 days old from the start of inflation. The white circle in the top panel and the pink circle in the bottom panel indicate the pulsar position.

remnant. Because of their compactness, PWNe in gamma-ray binaries acquire characteristic flow patterns and accumulate energy much more rapidly than their remnant counterparts. They easily adjust their flow pattern to local conditions in the stellar

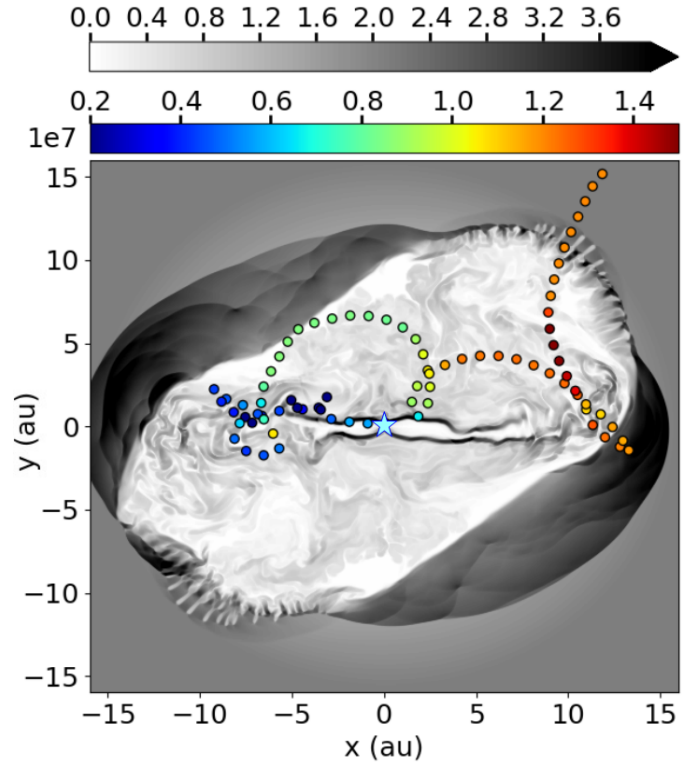


Fig. 3. Trajectory and energy gain of an accelerating proton with an initial energy $2.4 \times 10^{15} \text{ eV}$. The test-particle proton were injected near the pulsar wind termination shock into the wind collision region. The trajectory is traced by thick dots, and the gain (in terms of the Lorentz factor) is shown by the color of the dots. The trajectory is modeled using a time-dependent model, but for clarity it is superimposed on a still map of the system's magnetic field B (in G; top gray color bar); the blue star indicates the pulsar position. As can be seen, the proton left the system, gaining energy above 10^{16} eV , after several scatterings in a mildly relativistic MHD flow. The system of colliding winds is simulated for a stellar wind magnetic field of 2 G and a pulsar spin-down luminosity of $10^{37} \text{ erg} \cdot \text{s}^{-1}$ (model C in Table 1). The brightness scale of the map is adjusted to highlight the structure of RMHD outflows and does not reflect the maximum and minimum values of B in the system. The map shows the system 0.56 days old since its inflation began.

wind anywhere in the pulsar's orbit, especially when the pulsar is crossing (or traveling in) the dense, highly-magnetized equatorial disk of a massive star. Actually, the evolution of MHD flows in PWNe and the acceleration of PeV protons in these flows occur on comparable time scales (from a few, up to several hours). This allows one to limit the modeling of PeV protons acceleration to a short local part of the orbit, which is essentially what we do: we consider the *local* structure of a wind collision region on time scales of the order of $\sim 10^5$ sec. This also suggests, as a first approximation, that the pulsar nebula sees the surrounding stellar wind as a plane, homogeneous flow. Moreover, if this flow carries a magnetic field of the Gauss-range, then it will most likely to be controlled by this field, so that the field of velocity and the magnetic field in this flow can be considered to a fairly good approximation as co-directional.

The accelerated particles could reach higher energies if a more complex model of the clumpy wind of a massive star were considered. The presence of clumps in a stellar wind in gamma-

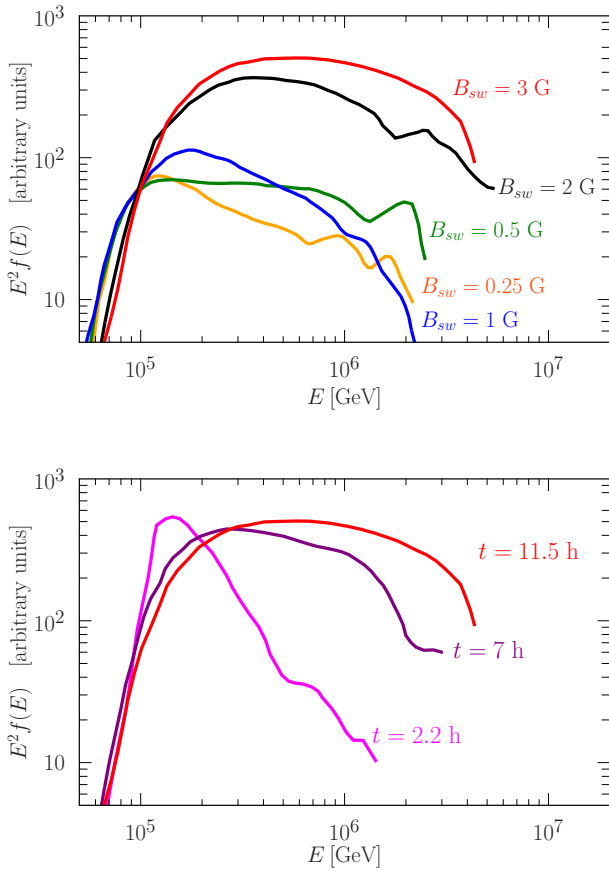


Fig. 4. Spectral energy distributions of PeV-regime protons accelerating in a gamma-ray binary system, in models from E to I in Table 1. Shown are the spectra of particles inside the simulation domain. Top graph: Spectra of accelerating particles at different strengths of the stellar wind magnetic field B_{sw} (in Gauss units): 0.25 – orange curve, 0.5 – green, 1 – blue, 2 – black, 3 – red. In the illustration, spectra were smoothed and taken in a system that had evolved from scratch for 18.5 hours, and 11.5 h after the particles were injected into the system. Bottom graph: Spectra of accelerating particles at different moments in the evolution of the system. In the illustration, we show the moments $t = 2.2$ (magenta), 7 (purple) and 11.5 (red) hours after the injection of test particles for model I , $B_{sw} = 3$ G.

ray binary systems hosting a Be-star and a pulsar is consistent with multiwavelength observations (see e.g. Owocki et al., 2009; Bosch-Ramon, 2013; Chernyakova et al., 2020b; Kefala & Bosch-Ramon, 2023; Yoneda et al., 2023). Density clumps and corresponding magnetic inhomogeneities can significantly influence the energy distribution of PeV-regime particles, leading to a hardening of their spectrum. Accounting for the clumps would require much more computational resources than the current model consumes, so we will leave this for a dedicated study of the issue. In a model way, this issue was addressed in Monte Carlo simulation by Bykov et al. (2021). They examined the effect of scattering of cosmic rays by magnetic inhomogeneities (clumps in the wind of a massive star) in colliding winds in the gamma-ray binary PSR J2032+4127/MT91 213 and showed that it can lead to a hard spectrum of PeV particles and maximum energies of accelerated protons above 10 PeV. Monte Carlo modeling assumed a parameterization of particle

scattering rate. Here by means of direct simulation of particle trajectories in magnetohydrodynamic flow produced by the colliding winds we showed that PeV-regime particles can be accelerated even in a simplified system modeled as an asymptotically homogeneous magnetized stellar wind flow colliding with a pulsar wind.

The acceleration of protons above 10 PeV, which we observed in our simulations, is of particular interest because such particles can exceed the threshold of the photo-meson reaction (see e.g. Aharonian, 2004; Dermer & Menon, 2009) on seed photons of optical/ultraviolet radiation from a bright young massive star. This process could allow gamma-ray binaries to produce neutrinos and photons with energies above 100 TeV (see e.g. Neronov & Ribordy, 2009; Bykov et al., 2021). Recently, a ~ 150 TeV neutrino event associated with gamma-ray photons with energies above 300 TeV have been reported. Both signals originated from the Cygnus region containing PSR J2032+4127/MT91 213 and Cyg X3 (Dzhappuev et al., 2021), suggesting a multi-PeV proton acceleration regime if the signals are associated with the gamma-ray binary system (Bykov et al., 2021).

There is evidence for the possible presence of a component of galactic origin among detected high-energy neutrino events (see e.g. Neronov & Semikoz, 2016; Troitsky, 2021; Kovalev et al., 2022). Note that accompanying $\gtrsim 300$ TeV gamma-rays cannot be detected from far away extragalactic sources (see Nikishov, 1962; Aharonian, 2004). The sub-population of gamma-ray binaries discussed above could contribute to the production of PeV-regime cosmic rays and be responsible for some of the neutrino events in the Milky Way.

There is about a dozen of confirmed gamma-ray binaries and in some of these the compact companion is a pulsar as we assumed above. Gauss-range magnetic field that is needed to accelerate PeV CRs, seems to be present in the winds interaction region in sources with the orbital periods shorter than a year. The binary sources with much longer orbital periods like the recently discovered PSR J2032+4127 can accelerate PeV particles during a short part of the period near the periastron. On the other hand the number of such sources can be larger than we currently know because their TeV appearance is not very frequent. The observed luminosity of TeV radiation in PSR J2032+4127 around the orbit periastron is about 10^{33} erg s^{-1} (Abeysekera et al., 2018; Katayose & Tibet ASgamma Collaboration, 2022). Models of the TeV radiation of gamma-ray binaries (see e.g. Chen et al., 2019; Takata et al., 2017) considered multi-TeV leptons as the main source of the observed TeV regime radiation. The efficiency of the gamma-ray radiation due to hadronic collisions in the close vicinity of the wind collision region is not necessarily very high allowing the power of the accelerated particles production to be much higher than the detected gamma-ray emission. It should be noted, however that the photo-hadronic radiation process at very high energies can be very efficient (see e.g. Aharonian, 2004; Neronov & Ribordy, 2009; Bykov et al., 2021). While the observational constrains on the hadronic components in this systems are not yet available, nevertheless a simplified Monte Carlo modeling Bykov et al. (2021) which assumed some TeV proton injection

rate into the wind colliding flows provided a high PeV proton acceleration efficiency. A non-negligible fraction of the plasma flows power can be transferred to PeV regime protons. Therefore, from the rough estimations the production power of the PeV regime CRs by the dozen of known gamma-ray binaries may reach $\sim 10^{36}$ erg s^{-1} .

The power of the CR sources needed to maintain the directly observed fluxes of CR nuclei at the Earth orbit in the PeV regime estimated by Murase & Fukugita (2019); Sudoh & Beacom (2023) is $\sim 10^{38}$ erg s^{-1} at 1 PeV. They got this CR production rate within a quasi-steady galactic CR propagation model. The estimation was obtained assuming that:

(i) the CRs of energies above PeV are distributed within the Galaxy in the same way as that of GeV-TeV CRs and

(ii) the confinement time of the PeV regime CRs can be obtained from the extrapolations of the traversed grammage of GeV-TeV nuclei which is derived from the detailed measurements of their isotopic composition.

While the gamma-ray maps and photon spectra obtained from the Milky Way with Fermi LAT detector are consistent with rather smooth CRs distribution over the Galaxy it remains to be proved with very high energy gamma-ray telescopes that the same is true for PeV regime CRs and their source distribution. At the moment PeV gamma-astronomy is the most perspective way to search the pevatrons. The gamma-ray binaries with high magnetic field detected by the current generation of TeV-PeV regime Cherenkov telescopes may be among a few sources that can be detected by the dedicated PeV gamma-ray observatories – LHAASO (Cao et al., 2021), TAIGA (Budnev et al., 2022) and the others. Galactic Pevatrons – sources of cosmic rays in the PeV-range – are still being sought among objects of various types (see e.g. Aharonian et al., 2019; Bykov et al., 2020; Amato & Casanova, 2021; Sudoh & Beacom, 2023), and gamma-ray and neutrinos observation will help to estimate the relative role of the different type PeV CRs sources.

5. Summary

The main goal of our work is to study the ability of gamma-ray binaries to accelerate multi-PeV energy cosmic rays, which may be responsible for gamma-ray and possibly high-energy neutrino emission of these systems. We injected protons which are assumed to be pre-accelerated to energies below the pulsar's potential drop (either by a rotation-powered pulsar or by some other process in the stellar winds) into time dependent domain with the colliding wind flows of highly magnetized plasma in the binary simulated with 2D RMHD model. Then we followed the trajectories of the injected particles by directly integrating their equations of motion (with 3D momenta) to study particle confinement and acceleration in a time-dependent system of the colliding MHD flows. The acceleration rate of PeV particles strongly depends on the magnitude of the magnetic field carried by the wind of the massive young star. If this magnitude is in the Gauss-range, then binaries hosting a pulsar with a spin-down luminosity above 10^{35} erg s^{-1} can accelerate protons to PeV energy regime (well above the potential drop energy of an isolated fast rotating pulsar) and radiate very high

energy photons and neutrinos. The contribution of this type of pevatrons to the observed galactic cosmic ray fluxes depends on the number of the gamma-ray binaries which is not yet certain having in mind the presence of long orbital period binaries like the recently discovered PSR J2032+4127. However, this object can be considered as a candidate source of PeV regime radiation from the Cygnus region reported by LHAASO (Cao et al., 2021) and Carpet 2 (Dzhappuev et al., 2021). Another perspective objects for a search of the very high energy radiation are LSI +61° 303 and LS 5039. The nature of a compact companion in gamma-ray binary LS 5039 is not yet established, but the presence of hard X-rays - soft gamma rays synchrotron component with a very hard spectral index (Falanga et al., 2021) may indicate the presence of colliding winds in the short period gamma-ray binary.

6. Acknowledgments

The authors thank the two referees for constructive and useful comments. This research made use of PLUTO public RMHD code developed by A. Mignone and the PLUTO team. We acknowledge the use of data provided by NASA ADS system and SIMBAD database, operated at CDS, Strasbourg, France. Simulations were performed partly at the Joint Supercomputer Center JSCC of the Russian Academy of Sciences, and partly at the *Tornado* subsystem of the Supercomputing Center at the Peter the Great Saint-Petersburg Polytechnic University. Cosmic ray particle spectra simulations by A.M.B. and A.E.P. were supported by the RSF grant 21-72-20020. Pulsar wind nebula model setup was made by K.P.L. and G.A.P. who were supported by the baseline project at the Ioffe Institute.

References

- Abaroa, L., Romero, G. E., & Sotomayor, P. (2023). Supercritical colliding wind binaries. *Astron. Astrophys.*, 671, A9. doi:10.1051/0004-6361/202245285. arXiv:2301.08635.
- Abeysekara, A. U., Albert, A., Alfaro, R. et al. (2021). HAWC observations of the acceleration of very-high-energy cosmic rays in the Cygnus Cocoon. *Nature Astronomy*, 5, 465–471. doi:10.1038/s41550-021-01318-y. arXiv:2103.06820.
- Abeysekara, A. U., Benbow, W., Bird, R. et al. (2018). Periastron Observations of TeV Gamma-Ray Emission from a Binary System with a 50-year Period. *ApJ Lett.*, 867(1), L19. doi:10.3847/2041-8213/aae70e. arXiv:1810.05271.
- Ackermann, M., Ajello, M., Allafort, A. et al. (2011). A Cocoon of Freshly Accelerated Cosmic Rays Detected by Fermi in the Cygnus Superbubble. *Science*, 334, 1103–. doi:10.1126/science.1210311.
- Aharonian, F., Akhperjanian, A., Beilicke, M. et al. (2002). An unidentified TeV source in the vicinity of Cygnus OB2. *Astron. Astrophys.*, 393, L37–L40. doi:10.1051/0004-6361:20021171. arXiv:astro-ph/0207528.
- Aharonian, F., Yang, R., & de Oña Wilhelmi, E. (2019). Massive stars as major factories of Galactic cosmic rays. *Nature Astronomy*, 3, 561–567. doi:10.1038/s41550-019-0724-0. arXiv:1804.02331.
- Aharonian, F. A. (2004). *Very high energy cosmic gamma radiation : a crucial window on the extreme Universe*, World Scientific Publishing Co. doi:10.1142/4657.
- Amato, E., & Arons, J. (2006). Heating and Nonthermal Particle Acceleration in Relativistic, Transverse Magnetosonic Shock Waves in Proton-Electron-Positron Plasmas. *ApJ*, 653(1), 325–338. doi:10.1086/508050. arXiv:astro-ph/0609034.

- Amato, E., & Casanova, S. (2021). On particle acceleration and transport in plasmas in the Galaxy: theory and observations. *Journal of Plasma Physics*, 87(1), 845870101. doi:10.1017/S0022377821000064. arXiv:2104.12428.
- Archambault, S., Archer, A., Aune, T. et al. (2016). Exceptionally Bright TeV Flares from the Binary LS I +61 303. *ApJ Lett.*, 817(1), L7. doi:10.3847/2041-8205/817/1/L7. arXiv:1601.01812.
- Arons, J. (2003). Magnetars in the Metagalaxy: An Origin for Ultra-High-Energy Cosmic Rays in the Nearby Universe. *ApJ*, 589(2), 871–892. doi:10.1086/374776. arXiv:astro-ph/0208444.
- Arons, J. (2012). Pulsar Wind Nebulae as Cosmic Pevatrons: A Current Sheet's Tale. *Space Sci. Rev.*, 173(1–4), 341–367. doi:10.1007/s11214-012-9885-1. arXiv:1208.5787.
- Ball, L., & Kirk, J. G. (2000). Probing pulsar winds using inverse Compton scattering. *Astroparticle Physics*, 12(4), 335–349. doi:10.1016/S0927-6505(99)00112-7. arXiv:astro-ph/9908201.
- Blandford, R., & Eichler, D. (1987). Particle acceleration at astrophysical shocks: A theory of cosmic ray origin. *Physics Reports*, 154, 1–75.
- Bosch-Ramon, V. (2013). Clumpy stellar winds and high-energy emission in high-mass binaries hosting a young pulsar. *Astron. Astrophys.*, 560, A32. doi:10.1051/0004-6361/201322249. arXiv:1310.5641.
- Bosch-Ramon, V., Barkov, M. V., Khangulyan, D., & Perucho, M. (2012). Simulations of stellar/pulsar-wind interaction along one full orbit. *Astron. Astrophys.*, 544, A59. doi:10.1051/0004-6361/201219251. arXiv:1203.5528.
- Budnev, N. M., Kuzmichev, L., Mirzoyan, R. et al. (2022). TAIGA - an advanced hybrid detector complex for astroparticle physics, cosmic ray physics and gamma-ray astronomy. In *37th International Cosmic Ray Conference* (p. 731). doi:10.22323/1.395.0731. arXiv:2208.13757.
- Bykov, A., Gehrels, N., Krawczynski, H., Lemoine, M., Pelletier, G., & Pohl, M. (2012). Particle Acceleration in Relativistic Outflows. *Space Sci. Rev.*, 173, 309–339. arXiv:1205.2208.
- Bykov, A. M., Amato, E., Petrov, A. E., Krassilchtchikov, A. M., & Levenfish, K. P. (2017). Pulsar Wind Nebulae with Bow Shocks: Non-thermal Radiation and Cosmic Ray Leptons. *Space Sci. Rev.*, 207, 235–290. doi:10.1007/s11214-017-0371-7. arXiv:1705.00950.
- Bykov, A. M., Ellison, D. C., Marcowith, A., & Osipov, S. M. (2018). Cosmic Ray Production in Supernovae. *Space Sci. Rev.*, 214(1), 41. doi:10.1007/s11214-018-0479-4. arXiv:1801.08890.
- Bykov, A. M., Marcowith, A., Amato, E., Kalyashova, M. E., Kruijssen, J. M. D., & Waxman, E. (2020). High-Energy Particles and Radiation in Star-Forming Regions. *Space Sci. Rev.*, 216(3), 42. doi:10.1007/s11214-020-00663-0. arXiv:2003.11534.
- Bykov, A. M., Petrov, A. E., Kalyashova, M. E., & Troitsky, S. V. (2021). PeV Photon and Neutrino Flares from Galactic Gamma-Ray Binaries. *ApJ Lett.*, 921(1), L10. doi:10.3847/2041-8213/ac2f3d. arXiv:2110.11189.
- Cao, Z., Aharonian, F. A., An, Q. et al. (2021). Ultrahigh-energy photons up to 1.4 petaelectronvolts from 12 γ -ray Galactic sources. *Nature*, 594(7861), 33–36. doi:10.1038/s41586-021-03498-z.
- Casares, J., Ribó, M., Ribas, I., Paredes, J. M., Martí, J., & Herrero, A. (2005). A possible black hole in the γ -ray microquasar LS 5039. *MNRAS*, 364(3), 899–908. doi:10.1111/j.1365-2966.2005.09617.x. arXiv:astro-ph/0507549.
- Cerutti, B., Philippov, A. A., & Dubus, G. (2020). Dissipation of the striped pulsar wind and non-thermal particle acceleration: 3D PIC simulations. *Astron. Astrophys.*, 642, A204. doi:10.1051/0004-6361/202038618. arXiv:2008.11462.
- Chen, A. M., Takata, J., Yi, S. X., Yu, Y. W., & Cheng, K. S. (2019). Modelling multiwavelength emissions from PSR B1259-63/LS 2883: Effects of the stellar disc on shock radiations. *Astron. Astrophys.*, 627, A87. doi:10.1051/0004-6361/201935166. arXiv:1904.07527.
- Chernyakova, M., Malyshev, D., Blay, P., van Soelen, B., & Tsygankov, S. (2020a). Multiwavelength observations of PSR J2032+4127 during the 2017 periastron passage. *MNRAS*, 495(1), 365–374. doi:10.1093/mnras/staa1181. arXiv:2004.11884.
- Chernyakova, M., Malyshev, D., Mc Keague, S., van Soelen, B., Marais, J. P., Martin-Carrillo, A., & Murphy, D. (2020b). New insight into the origin of the GeV flare in the binary system PSR B1259-63/LS 2883 from the 2017 periastron passage. *MNRAS*, 497(1), 648–655. doi:10.1093/mnras/staa1876. arXiv:2005.14060.
- Cristofari, P. (2021). The Hunt for Pevatrons: The Case of Supernova Remnants. *Universe*, 7(9), 324. doi:10.3390/universe7090324.
- De Becker, M., & Raucq, F. (2013). Catalogue of particle-accelerating colliding-wind binaries. *Astron. Astrophys.*, 558, A28. doi:10.1051/0004-6361/201322074. arXiv:1308.3149.
- de Oña Wilhelmi, E., López-Coto, R., Amato, E., & Aharonian, F. (2022). On the Potential of Bright, Young Pulsars to Power Ultrahigh Gamma-Ray Sources. *ApJ Lett.*, 930(1), L2. doi:10.3847/2041-8213/ac66cf. arXiv:2204.09440.
- Del Zanna, L., & Olmi, B. (2017). Multidimensional Relativistic MHD Simulations of Pulsar Wind Nebulae: Dynamics and Emission. In D. F. Torres (Ed.), *Modelling Pulsar Wind Nebulae* (p. 215). volume 446 of *Astrophysics and Space Science Library*. doi:10.1007/978-3-319-63031-1_10. arXiv:1703.10442.
- Dermer, C. D., & Menon, G. (2009). *High Energy Radiation from Black Holes: Gamma Rays, Cosmic Rays, and Neutrinos*. Princeton U. Press.
- Dubus, G. (2013). Gamma-ray binaries and related systems. *Astron. Astrophys. Rev.*, 21, 64. doi:10.1007/s00159-013-0064-5. arXiv:1307.7083.
- Dzhappuev, D. D., Afashokov, Y. Z., Dzaparova, I. M., et al. (2021). Observation of Photons above 300 TeV Associated with a High-energy Neutrino from the Cygnus Region. *ApJ Lett.*, 916(2), L22. doi:10.3847/2041-8213/ac14b2. arXiv:2105.07242.
- Eichler, D., & Usov, V. (1993). Particle Acceleration and Nonthermal Radio Emission in Binaries of Early-Type Stars. *ApJ*, 402, 271. doi:10.1086/172130.
- Falanga, M., Bykov, A. M., Li, Z., Krassilchtchikov, A. M., Petrov, A. E., & Bozzo, E. (2021). Phase-resolved hard X-ray emission of the high-mass binary LS 5039: a spectral hardening above 50 keV detected with INTEGRAL. *arXiv e-prints*, (p. arXiv:2104.07711). doi:10.1051/0004-6361/202141102. arXiv:2104.07711.
- Fiori, M., Olmi, B., Amato, E., Bandiera, R., Bucciantini, N., Zampieri, L., & Burdovoi, A. (2022). Modelling the γ -ray pulsar wind nebulae population in our galaxy. *MNRAS*, 511(1), 1439–1453. doi:10.1093/mnras/stac019. arXiv:2201.02221.
- Gaensler, B. M., & Slane, P. O. (2006). The Evolution and Structure of Pulsar Wind Nebulae. *Ann. Rev. Astron. Astrophys.*, 44(1), 17–47. doi:10.1146/annurev.astro.44.051905.092528. arXiv:astro-ph/0601081.
- Grimaldo, E., Reimer, A., Kissmann, R., Niederwanger, F., & Reitberger, K. (2019). Proton Acceleration in Colliding Stellar Wind Binaries. *ApJ*, 871(1), 55. doi:10.3847/1538-4357/aaf6ee. arXiv:1812.02960.
- Grunhut, J. H., Wade, G. A., Neiner, C. et al. (2017). The MiMeS survey of Magnetism in Massive Stars: magnetic analysis of the O-type stars. *MNRAS*, 465(2), 2432–2470. doi:10.1093/mnras/stw2743. arXiv:1610.07895.
- Guépin, C., Cerutti, B., & Kotera, K. (2020). Proton acceleration in pulsar magnetospheres. *Astron. Astrophys.*, 635, A138. doi:10.1051/0004-6361/201936816. arXiv:1910.11387.
- Hare, J., Kargaltsev, O., Pavlov, G., & Beniamini, P. (2019). Evolution of the Extended X-Ray Emission from the PSR B1259-63/LS 2883 Binary in the 2014–2017 Binary Cycle. *ApJ*, 882(2), 74. doi:10.3847/1538-4357/ab3648. arXiv:1905.12833.
- Ho, W. C. G., Ng, C. Y., Lyne, A. G., Stappers, B. W., Coe, M. J., Halpern, J. P., Johnson, T. J., & Steele, I. A. (2017). Multiwavelength monitoring and X-ray brightening of Be X-ray binary PSR J2032+4127/MT91 213 on its approach to periastron. *MNRAS*, 464(1), 1211–1219. doi:10.1093/mnras/stw2420. arXiv:1609.06328.
- Huber, D., Kissmann, R., Reimer, A., & Reimer, O. (2021). Relativistic fluid modelling of gamma-ray binaries. I. The model. *Astron. Astrophys.*, 646, A91. doi:10.1051/0004-6361/202039277. arXiv:2012.04975.
- Hubrig, S., Järvinen, S. P., Ilyin, I., Schöller, M., & Jayaraman, R. (2023). Are magnetic fields universal in O-type multiple systems? *MNRAS*, 521(4), 6228–6246. doi:10.1093/mnras/stad730. arXiv:2303.14791.
- Katayose, Y., & Tibet ASgamma Collaboration (2022). Gamma-ray Observation of the Cygnus Region with the Tibet Air Shower Array. In *37th International Cosmic Ray Conference* (p. 799). doi:10.22323/1.395.0799.
- Kefala, E., & Bosch-Ramon, V. (2023). Modeling the effects of clumpy winds in the high-energy light curves of γ -ray binaries. *Astron. Astrophys.*, 669, A21. doi:10.1051/0004-6361/202244531. arXiv:2210.16102.
- Klement, R., Carciofi, A. C., Rivinius, T., Matthews, L. D., Vieira, R. G., Ignace, R., Bjorkman, J. E., Mota, B. C., Faes, D. M., Bratcher, A. D., Curé, M., & Štefl, S. (2017). Revealing the structure of the outer disks of Be stars. *Astron. Astrophys.*, 601, A74. doi:10.1051/0004-6361/201629932. arXiv:1703.07321.

- Kobulnicky, H. A., Chick, W. T., & Povich, M. S. (2019). Mass-loss Rates for O and Early B Stars Powering Bow Shock Nebulae: Evidence for Bistability Behavior. *Astron. J.*, 158(2), 73. doi:10.3847/1538-3881/ab2716.
- Komissarov, S. S. (2013). Magnetic dissipation in the Crab nebula. *MNRAS*, 428(3), 2459–2466. doi:10.1093/mnras/sts214. arXiv:1207.3192.
- Kotera, K., Amato, E., & Blasi, P. (2015). The fate of ultrahigh energy nuclei in the immediate environment of young fast-rotating pulsars. *J. Cosmol. Astropart. Phys.*, 2015(8), 026–026. doi:10.1088/1475-7516/2015/08/026. arXiv:1503.07907.
- Kovalev, Y. Y., Plavin, A. V., & Troitsky, S. V. (2022). Galactic Contribution to the High-energy Neutrino Flux Found in Track-like IceCube Events. *ApJ Lett.*, 940(2), L41. doi:10.3847/2041-8213/aca1ae. arXiv:2208.08423.
- Lemaster, M. N., Stone, J. M., & Gardiner, T. A. (2007). Effect of the Coriolis Force on the Hydrodynamics of Colliding-Wind Binaries. *ApJ*, 662(1), 582–595. doi:10.1086/515431. arXiv:astro-ph/0702425.
- Lemoine, M., Kotera, K., & Pétri, J. (2015). On ultra-high energy cosmic ray acceleration at the termination shock of young pulsar winds. *J. Cosmol. Astropart. Phys.*, 2015(7), 016–016. doi:10.1088/1475-7516/2015/07/016. arXiv:1409.0159.
- Lyubarsky, Y. E. (2003). The termination shock in a striped pulsar wind. *MNRAS*, 345(1), 153–160. doi:10.1046/j.1365-8711.2003.06927.x. arXiv:astro-ph/0306435.
- Malkov, M., & Lemoine, M. (2023). Particle acceleration in colliding winds: Binary star winds and other double-shock structures. *Phys. Rev. E*, 107(2), 025201. doi:10.1103/PhysRevE.107.025201. arXiv:2212.08788.
- Mignone, A., Bodo, G., Massaglia, S., Matsakos, T., Tesileanu, O., Zanni, C., & Ferrari, A. (2007). PLUTO: A Numerical Code for Computational Astrophysics. *Astrophys. J. Suppl. Ser.*, 170(1), 228–242. doi:10.1086/513316. arXiv:astro-ph/0701854.
- Mignone, A., Bodo, G., Vaidya, B., & Mattia, G. (2018). A Particle Module for the PLUTO Code. I. An Implementation of the MHD-PIC Equations. *ApJ*, 859(1), 13. doi:10.3847/1538-4357/aabccd. arXiv:1804.01946.
- Molina, E., & Bosch-Ramon, V. (2020). A dynamical and radiation semi-analytical model of pulsar-star colliding winds along the orbit: Application to LS 5039. *Astron. Astrophys.*, 641, A84. doi:10.1051/0004-6361/202038417. arXiv:2007.00543.
- Murase, K., & Fukugita, M. (2019). Energetics of high-energy cosmic radiations. *Phys. Rev. D*, 99(6), 063012. doi:10.1103/PhysRevD.99.063012. arXiv:1806.04194.
- Neronov, A., & Ribordy, M. (2009). Neutrino signal from γ -ray-loud binaries powered by high energy protons. *Phys. Rev. D*, 79(4), 043013. doi:10.1103/PhysRevD.79.043013. arXiv:0812.0306.
- Neronov, A., & Semikoz, D. (2016). Evidence the Galactic contribution to the IceCube astrophysical neutrino flux. *Astroparticle Physics*, 75, 60–63. doi:10.1016/j.astropartphys.2015.11.002. arXiv:1509.03522.
- Ng, C. Y., Ho, W. C. G., Gotthelf, E. V., Halpern, J. P., Coe, M. J., Stappers, B. W., Lyne, A. G., Wood, K. S., & Kerr, M. (2019). X-Ray and Radio Variabilities of PSR J2032+4127 near Periastron. *ApJ*, 880(2), 147. doi:10.3847/1538-4357/ab2adb. arXiv:1907.05749.
- Nikishov, A. (1962). Absorption of high-energy photons in the Universe. *Sov. Phys. JETP*, 14, 393.
- Owocki, S. P., Romero, G. E., Townsend, R. H. D., & Araudo, A. T. (2009). Gamma-Ray Variability from Wind Clumping in High-Mass X-Ray Binaries with Jets. *ApJ*, 696(1), 690–693. doi:10.1088/0004-637X/696/1/690. arXiv:0902.2278.
- Pittard, J. M., Romero, G. E., & Vila, G. S. (2021). Particle acceleration and non-thermal emission in colliding-wind binary systems. *MNRAS*, 504(3), 4204–4225. doi:10.1093/mnras/stab1107. arXiv:2104.07399.
- Porth, O., Buehler, R., Olmi, B., Komissarov, S., Lamberts, A., Amato, E., Yuan, Y., & Rudy, A. (2017). Modelling Jets, Tori and Flares in Pulsar Wind Nebulae. *Space Sci. Rev.*, 207(1-4), 137–174. doi:10.1007/s11214-017-0344-x. arXiv:1703.05184.
- Porth, O., Komissarov, S. S., & Keppens, R. (2014). Three-dimensional magnetohydrodynamic simulations of the Crab nebula. *MNRAS*, 438(1), 278–306. doi:10.1093/mnras/stt2176. arXiv:1310.2531.
- Ressler, S. M. (2021). 3D MHD simulation of a pulsationally driven MRI accretion disc. *MNRAS*, 508(4), 4887–4901. doi:10.1093/mnras/stab2880. arXiv:2110.03693.
- Reynolds, S. P., Pavlov, G. G., Kargaltsev, O., Klingler, N., Renaud, M., & Mereghetti, S. (2017). Pulsar-Wind Nebulae and Magnetar Outflows: Observations at Radio, X-Ray, and Gamma-Ray Wavelengths. *Space Sci. Rev.*, 207(1-4), 175–234. doi:10.1007/s11214-017-0356-6. arXiv:1705.08897.
- Rivinius, T., Carciofi, A. C., & Martayan, C. (2013). Classical Be stars. Rapidly rotating B stars with viscous Keplerian accretion disks. *Astron. Astrophys. Rev.*, 21, 69. doi:10.1007/s00159-013-0069-0. arXiv:1310.3962.
- Romero, G. E., Boettcher, M., Markoff, S., & Tavecchio, F. (2017). Relativistic Jets in Active Galactic Nuclei and Microquasars. *Space Sci. Rev.*, 207(1-4), 5–61. doi:10.1007/s11214-016-0328-2. arXiv:1611.09507.
- Shannon, R. M., Johnston, S., & Manchester, R. N. (2014). The kinematics and orbital dynamics of the PSR B1259-63/LS 2883 system from 23 yr of pulsar timing. *MNRAS*, 437(4), 3255–3264. doi:10.1093/mnras/stt2123. arXiv:1311.0588.
- Shultz, M. E., Wade, G. A., Rivinius, T., Alecian, E., Neiner, C., Petit, V., Owocki, S., ud-Doula, A., Kochukhov, O., Bohlender, D., Keszhelyi, Z., MiMeS Collaboration, & BinaMiCS Collaboration (2019). The magnetic early B-type stars - III. A main-sequence magnetic, rotational, and magnetospheric biography. *MNRAS*, 490(1), 274–295. doi:10.1093/mnras/stz2551. arXiv:1909.02530.
- Sudoh, T., & Beacom, J. F. (2023). Where are Milky Way's hadronic PeVatrons? *Phys. Rev. D*, 107(4), 043002. doi:10.1103/PhysRevD.107.043002. arXiv:2209.03970.
- Takata, J., Tam, P. H. T., Ng, C. W., Li, K. L., Kong, A. K. H., Hui, C. Y., & Cheng, K. S. (2017). High-energy Emissions from the Pulsar/Be Binary System PSR J2032+4127/MT91 213. *ApJ*, 836(2), 241. doi:10.3847/1538-4357/aa5c80. arXiv:1702.04446.
- Tavani, M., & Arons, J. (1997). Theory of High-Energy Emission from the Pulsar/Be Star System PSR 1259-63. I. Radiation Mechanisms and Interaction Geometry. *ApJ*, 477(1), 439–464. doi:10.1086/303676. arXiv:astro-ph/9609086.
- Tibet ASy Collaboration, Amenomori, M., Bao, Y. W. et al. (2021). Potential PeVatron supernova remnant G106.3+2.7 seen in the highest-energy gamma rays. *Nature Astronomy*, 5, 460–464. doi:10.1038/s41550-020-01294-9.
- Torres, D. F. (2011). γ -ray binaries as non-accreting pulsar systems. In *High-Energy Emission from Pulsars and their Systems* (p. 531). volume 21 of *Astrophysics and Space Science Proceedings*. arXiv:1008.0483.
- Troitsky, S. V. (2021). Constraints on models of the origin of high-energy astrophysical neutrinos. *Physics Uspekhi*, 64(12), 1261–1285. doi:10.3367/UFNe.2021.09.039062. arXiv:2112.09611.
- ud-Doula, A., & Owocki, S. (2022). Magnetically confined wind shock. *arXiv e-prints*, (p. arXiv:2209.08540). arXiv:2209.08540.
- Vieu, T., Gabici, S., & Tatischeff, V. (2020). Particle acceleration at colliding shock waves. *MNRAS*, 494(3), 3166–3176. doi:10.1093/mnras/staa799. arXiv:2003.03411.
- Weng, S.-S., Qian, L., Wang, B.-J., Torres, D. F., Papitto, A., Jiang, P., Xu, R., Li, J., Yan, J.-Z., Liu, Q.-Z., Ge, M.-Y., & Yuan, Q.-R. (2022). Radio pulsations from a neutron star within the gamma-ray binary LS I +61° 303. *Nature Astronomy*, 6, 698–702. doi:10.1038/s41550-022-01630-1. arXiv:2203.09423.
- Yoneda, H., Bosch-Ramon, V., Enoto, T., Khangulyan, D., Ray, P. S., Strohmer, T., Tamagawa, T., & Wadiasingh, Z. (2023). Unveiling Properties of the Nonthermal X-Ray Production in the Gamma-Ray Binary LS 5039 Using the Long-term Pattern of Its Fast X-Ray Variability. *ApJ*, 948(2), 77. doi:10.3847/1538-4357/acc175. arXiv:2303.12587.

Appendix A. RMHD model

The acceleration of PeV-range protons in gamma-ray binaries is modeled using the results of a 2D relativistic MHD simulation of the time-dependent structure of the wind collision region in these objects. The simulation is based on the *Relativistic MHD module* and the *Cosmic Ray particle module* of the code PLUTO (Mignone et al., 2007, 2018).

The simulation is carried out in the reference frame of the pulsar. At the beginning of each numerical run, we initiate a stationary uniform stellar wind flow with co-directional magnetic field and velocity, and fixed pressure and mass density.

The flow is initiated throughout the entire computational domain, with the exception of a small area with radius $r_{in} = 0.15$ AU around a pulsar. From this area the pulsar wind is injected. The pulsar wind model is described in Appendix B.

We employ 2D Cartesian grid evenly spaced in both dimensions. The parameters of the computational grids are given in Table 1. The smallest scales (~ 0.01 – 0.1 AU) allowed by the grid are 10^3 – 10^4 times larger than the radii of the light cylinder of pulsars in gamma-ray binary systems. Yet, in a small vicinity of the polar axis of a pulsar wind nebula, the adopted resolution may still be insufficient for the cusps of the pulsar wind termination shock to be fully detached from the area of pulsar wind injection. This may have a minor effect on the plasma dynamics in the vicinity of the shock funnels (interfering with the formation of jets in the nebula), but is unlikely to affect the structure of nebular flows at the scales of interest. In all runs, the boundary conditions of free outflow for a background plasma and free escape for particles are adopted.

The inclination of the pulsar's rotation axis to the magnetic axis is described by the angle α , and to the direction of the stellar wind magnetic field – by the angle ψ . In the present study we take $\psi = 45^\circ$ and $\alpha = 45^\circ$. The pulsar's inclination α and spin-down luminosity L , and the pulsar wind's initial magnetization σ_0 and Lorentz-factor Γ_w are free parameters of the pulsar wind model (see Appendix B). Together with the stellar wind parameters they are listed in Table 1. We consider a wide range of the massive star's magnetic fields and mass loss rates, and chose some reference values for the stellar wind magnetic field and number density (as described in Sec. 2). Some parameters whose values are considered fixed in all runs are given in the legend of Table 1.

For simplicity, we used the equation of state of an ideal plasma for the SW and neglected the radiative losses in simulation of local vicinities of colliding winds region. We also adopted a constant $\gamma = 4/3$ for the both winds, following a typical approach (see e.g., p.1.2.1 of Del Zanna & Olmi, 2017)

Appendix B. Pulsar wind model

We applied a pulsar wind model of Porth et al. (2014). The free parameters of the model are: the spin-down luminosity L and magnetic inclination α of the pulsar, and the Lorentz factor Γ_w and initial magnetization σ_0 of the pulsar wind. Their values are listed in Table 1.

The model assumes a latitudinally anisotropic wind with an energy flux density depending on colatitude θ and radial coordinate r as

$$f_{tot}(r, \theta) = \frac{L}{L_0} \frac{1}{r^2} \cdot (\sin^2 \theta + \varepsilon). \quad (3)$$

Here L is a pulsar spin-down luminosity, $L_0 = 4\pi(2/3 + \varepsilon)$ is a normalization constant, and $\varepsilon = 0.02$ prevents the energy flux from vanishing at the poles. The wind is cold, so its total energy flux is divided into magnetic and kinetic components, $f_{tot} = f_m + f_k$:

$$f_m(r, \theta) = \frac{\sigma(\theta) \cdot f_{tot}(r, \theta)}{1 + \sigma(\theta)}; \quad f_k(r, \theta) = \frac{f_{tot}(r, \theta)}{1 + \sigma(\theta)}. \quad (4)$$

run	B_{sw}, G	$\psi, ^\circ$	$L, \text{erg/s}$	σ_0	Γ_w	box, au^2	$N_x \times N_y$	Δ, au
A	0.1	45	10^{37}	3	100	40×40	1600×1600	0.025
B	1	45	10^{37}	3	100	40×40	1600×1600	0.025
C	2	45	10^{37}	3	100	40×40	1600×1600	0.025
D	3	45	10^{37}	3	100	40×40	1600×1600	0.025
E	0.25	45	10^{37}	0.3	100	40×40	1600×1600	0.025
F	0.5	45	10^{37}	0.3	100	40×40	1600×1600	0.025
G	1	45	10^{37}	0.3	100	40×40	1600×1600	0.025
H	2	45	10^{37}	0.3	100	40×40	1600×1600	0.025
I	3	45	10^{37}	0.3	100	40×40	1600×1600	0.025

Table 1. Numerical RMHD models of a gamma-ray binary system.

Computation domain:

“box” – size,

N_x, N_y – number of grid cells in the x, y directions

$\Delta = \Delta_x = \Delta_y$ – numerical resolution of a uniform Cartesian 2D grid.

Parameters of the pulsar wind model (see in Appendix):

Γ_w – the Lorentz factor,

L – spin-down luminosity,

σ_0 – initial magnetization,

$\alpha = 45^\circ$ – angle between the rotational and magnetic axes of the pulsar.

Parameters of the stellar wind model:

B_{sw} – magnetic field,

$v_{sw} = 300 \text{ km} \cdot \text{s}^{-1}$ – velocity,

$p_{sw} = 10^{-7} \text{ dyn} \cdot \text{cm}^{-2}$ – pressure,

$n_{sw} = 3 \cdot 10^4 \text{ cm}^{-3}$ – proton number density,

ψ – angle between the pulsar's rotational axis and B_{sw} .

Notes: An estimate of n_{sw} is given for the distance (from a Be-star) of 10^{14} au and the stellar mass loss rate $\dot{M}_{-7} \sim 0.01 M_\odot \cdot \text{yr}^{-1}$. An estimate of v_{sw} refers for a Be-star equatorial outflow velocity as seen in the pulsar's rest frame. A grid resolution Δ is suitable for studying the confinement and acceleration of very high energy particles of PeV regime.

The ratio f_m/f_k determines the wind magnetization σ (upstream of the termination shock) at a given colatitude θ :

$$\sigma(\theta) = \frac{\tilde{\sigma}(\theta) \cdot \chi_\alpha(\theta)}{1 + \tilde{\sigma}(\theta) \cdot (1 - \chi_\alpha(\theta))}. \quad (5)$$

The magnetic field of the pulsar wind is frozen into the plasma and purely toroidal. The toroidal field must vanish at the poles and change sign at the rotational equator of the pulsar. Eq. 5 accounts for these features with the functions $\tilde{\sigma}$ and χ , respectively:

$$\tilde{\sigma}(\theta) = \sigma_0 \cdot \min \left\{ 1, \theta^2/\theta_0^2, (\pi - \theta)^2/\theta_0^2 \right\}; \quad (6)$$

$$\chi_\alpha(\theta) = \begin{cases} (2\phi_a(\theta)/\pi - 1)^2 & \text{if } |\pi/2 - \theta| < \alpha \\ 1 & \text{otherwise} \end{cases}, \quad (7)$$

with $\phi_a(\theta) = \arccos(-\cot(\theta)\cot(\alpha))$. Here $\theta_0 = 10^\circ$, and σ_0 is an initial magnetization of the wind at the light cylinder of the pulsar. As a result of the sign change, the wind of a rotating pulsar with a magnetic inclination α carries stripes of alternating magnetic polarity, filling the equatorial sector of the wind with an angular extent of $\pm\alpha$. The stripes are supposed to annihilate, either on the way to the termination shock, or directly on it (Lyubarsky, 2003; Komissarov, 2013; Cerutti et al., 2020). Hence, within the striped wind sector subtended by an angle 2α , the magnetic field should dissipate completely, as described by Eqs. 5–7. In the simulation, we take $\alpha = 45^\circ$. The magnetic field and density are then calculated using Eq. (4):

$$B_{pw}(r, \theta) = \pm \sqrt{4\pi f_m(r, \theta)/c}, \quad \rho_{pw}(r, \theta) = \frac{f_k(r, \theta)}{\Gamma_w^2 c^3}. \quad (8)$$

The wind velocity is directed radially outwards; its magnitude in terms of the Lorentz-factor Γ_w is

$$u_{pw}/c = \sqrt{1 - \Gamma_w^{-2}}. \quad (9)$$

On the inner boundary of the wind, pressure is calculated using the equation of state for an ideal relativistic plasma (with the adiabatic index $\gamma = 4/3$). Radial and angular coordinates are expressed in terms of Cartesian coordinates as

$$r = \sqrt{x^2 + y^2}; \quad \theta = \arccos\left(y/\sqrt{x^2 + y^2}\right) \quad (10)$$

Appendix C. Test particle propagation

Propagation and acceleration of PeV-regime protons are simulated using the particle moving unit of the PLUTO code (*Cosmic Ray* module; Mignone et al., 2018). In this module the MHD-PIC model is implemented, and accelerating particles are treated with the particle-in-cell techniques. The latter allow one to resolve the particle gyration (Larmor) scales. In the setups A–D, 10,000 protons with an initial energy of 2.4 PeV are injected near the PWN boundary 1/6 day after the start of the PWN evolution. At this point, the nebula is already fully developed. After injection, protons are treated as test-particles that do not affect the dynamics of the background plasma. Their propagation is followed simultaneously with the flow dynamics using the MHD-PIC formalism implemented in PLUTO. To study the spectral evolution of the accelerated particles, in the setups E–I we inject 160,000 particles with an energy of 0.1 PeV.